Chalcogenide Letters Vol. 19, No. 5, May 2022 p. 353 - 361

Band gap determination of chemically deposited Cu_2S/Fe_2O_3 quaternary thin films

R. O. Okoro[a], C. Augustine[b, c*], R. A. Chikwenze[b], S. O. Amadi[b], P. N. Kalu[b], P.E. Okpani[d], B. J. Robert[e], O. N. Nwoke[f], K.O. Achilike[g], C. O. Dike[b]
[a]*Department of Physics, Ebonyi State College of Education, Ebonyi State, Nigeria*
[b]*Department of Physics, Alex Ekwueme Federal University Ndufu-Alike, Ebonyi State, Nigeria*
[c]*Department of Industrial Physics, King David University of Medical Sciences, Uburu, Ebonyi State, Nigeria*
[d]*Department of Electrical/Electronic Engineering, Alex Ekwueme Federal University Ndufu Alike, Ebonyi State, Nigeria*
[e]*Department of Electrical/Electronic Engineering Technology, Akanu Ibiam Federal Polytechnic, Unwana, Ebonyi State, Nigeria*
[f]*Department of Mechanical Engineering, Akanu Ibiam Federal Polytechnic, Unwana, Ebonyi State, Nigeria*
[g]*Department of Industrial Physics, Abia State University, Uturu, Abia State,Nigeria*

Quaternary thin films of Cu_2S/Fe_2O_3 have been synthesized via simple, inexpensive and highly reproducible chemical bath deposition technique. The grown films were characterized with Rutherford backscattering technique (RBS), X-ray diffractometer (XRD), scanning electron microscope (SEM), and spectrophotometer for compositional, structural, morphological, and optical properties respectively. The multiple peaks exhibited by the various XRD patterns of the films showed that the films are polycrystalline while the SEM analysis showed an increase in grain size and uniformity of grain distribution as temperature increases. The absorbance (A), transmittance (T), absorption coefficient (α), band gap (E_g), extinction coefficient (k), real (ε_r) and imaginary dielectric (ε_i) constants were modified by thermal annealing. The optical and solid state analysis for Cu_2S/Fe_2O_3 thin films indicate that $A \leq 0.66$, $T \leq 92$ %, $\alpha \leq 1.70 \times 10^6 m^{-1}$, E_g increases from 3.75-3.85 eV, $k \leq 3.75$, $\varepsilon_r \leq 8.5$ and $\varepsilon_i \leq 2.05$. The high transmittance in the infrared region of Cu_2S-Fe_2O_3 thin films deposited suggest that the films can be used as coating materials for the construction of poultry houses in order to protect young chicks which have not developed protective thick feather from UV radiation while admitting the heating portion of electromagnetic spectrum into the house for warming young chicks. Based on the wide band gap exhibited by all the quaternary thin films, they are promising materials for window layers in solar cell fabrication and fabrication of optoelectronic devices, etc.

(Received September 30, 2021; Accepted May 12, 2022)

Keywords: Band gap, Chemical bath, XRD, SEM, Transmittance

1. Introduction

Cu_2S semiconductor is a good material for solar energy absorber due to its character of non-toxic, low cost and ideal band gap of 1.2-2.5 eV [1]. Copper sulphide thin films are considered as promising materials for solar energy conversion as p-type semiconductor and absorber of visible light [2, 3]. On the other hand, Fe_2O_3 is the most stable oxide of iron and is environmentally friendly (non-toxic), highly resistant to corrosion and ferromagnetic [4]. It occurs naturally in the form of a mineral resource called hematite which is the major source of iron used

* Corresponding author: emmyaustine2003@yahoo.com
https://doi.org/10.15251/CL.2022.195.353

in producing steel [4]. In the form of fine powder, α-Fe_2O_3 is used in polishing metallic jewelry and lenses [5]. Alpha-Fe_2O_3 is used as catalyst for petrochemical applications [6] and also has biomedical applications [7,8].

The integration of Cu_2S and Fe_2O_3 components into quaternary thin films has the potential of tailoring the band gap for various applications. The survey of literature showed that both binary films have deposited by both physical and chemical deposition techniques. The chemical bath deposition his gained prominence due to the following factors: low deposition temperature, reproducibility, mass production of samples, availability of apparatus, etc. The chemical bath deposition involves two steps, nucleation and particle growth, and is based on the formation of a solid phase from a solution. In the chemical bath deposition procedure, the substrate is immersed in a solution containing the precursors. This method depends upon parameters like temperature, pH of the solution, molarities and time. The major advantage of CBD is that it requires in its simplest form only solution, containers and substrate mounting devices it yields stable, adherent, uniform and hard films with good reproducibility by a relatively simple process [9]. The growth of thin films strongly depends on growth conditions, such as duration of deposition, composition and temperature of the solution, and topographical and chemical nature of the substrate [10] .The formation of films takes place when ionic product exceeds solubility product (IP > SP) [11]. In view of the above facts, the aim of the present work is to deposit of Cu_2S/Fe_2O_3 quaternary thin films using chemical bath deposition method and characterize same for band gap determination.

2. Materials and methods

The deposition of Cu_2S/Fe_2O_3 quaternary thin films were done by first depositing Cu_2S films on clean glass substrates from chemical bath containing 3mls, 0.1M of $CuCl_2$, 2mls of 0.1M of $(NH_2)_2CS$, 4mls of 0.2M of $Na_2S_2O_3$ (complexing agent) and 7mls of distilled water at 60 ^oC bath temperature with pH of 9.7 for 90 minutes. Then, the glass substrates now coated with Cu_2S films were inserted into a chemical bath containing 10 mls, 0.5M of $FeSO_4.7H_2O$, 10mls of 0.5M of KCl, 2 drops of 1M of NaOH (source of hydroxyl ions) and 38mls of distilled water in that order with pH of 5.2 at 60 ^oC bath temperature for 2 hours. Rutherford backscattering (RBS) was used to determine the elemental compositions, depth profile and thicknesses of the films by Proton Induced X-ray Emission (PIXE) scans on the samples from a Tandem Accelerator Model 55DH 1.7MV Pellaton The crystal structure and phase analysis of the deposited film was carried out at room temperature with an X-ray diffractrometer Rigaku Ultima IV model, using gracing incident at 30 mA, 40KV with CuKα radiation of wavelength λ = 0.15406nm selected by a diffracted beam monochromator. The thin films were scanned continuously between 0^o to 90^o at a step size of 0.034 and at a time per step of 56.7s. The XRD diffractograms of intensity versus 2θ values were generated and displayed. Phase identification was then made from an analysis of intensity of peaks versus 2θ, using ICDD data. Thermo scientific GENESYS 10S model UV-VIS spectrophotometer was used to determine the absorbance of the deposited films in the wavelength range of 300-1000 nm

3. Result and discussion

The elemental components of Cu, S, Fe and O were quantitatively obtained from RBS analysis as shown in the micrograph (Fig.1). Other elements present could have come from the glass substrate and some impurities.

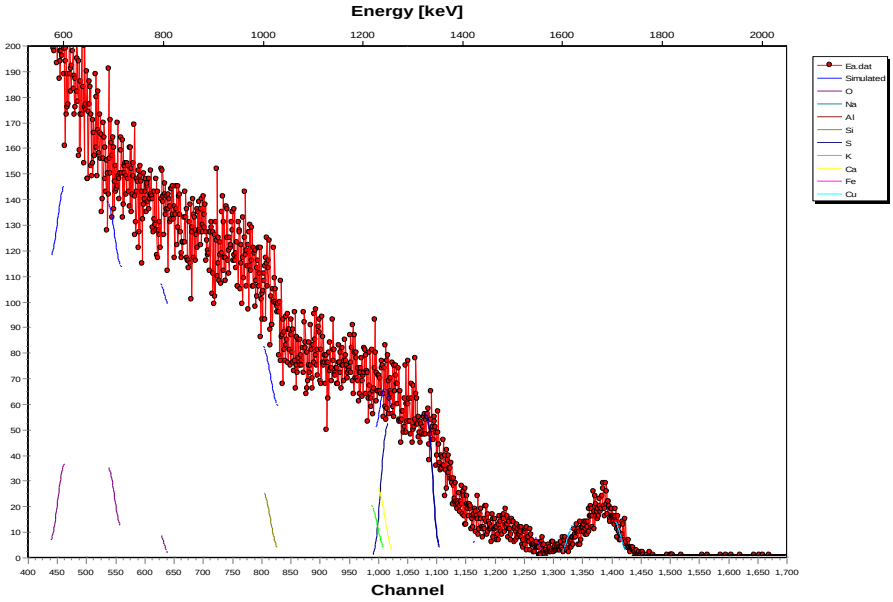

Fig. 1. RBS micrograph of Cu_2S/Fe_2O_3 quaternary thin films.

The peak angles of 28°, 32° and 47° with reflections (111), (200) and (220) are attributed to Cu_2S phase (JCPDS 65-2980) while angles of 25°, 33° and 37° corresponding to (012), (221) and (110) respectively are attributed Fe_2O_3 phase (JCPDS 87-1164). The films are polycrystalline based on the multiple peaks exhibited by the diffractograms. These findings are in agreement with the report of other research groups [12, 13].

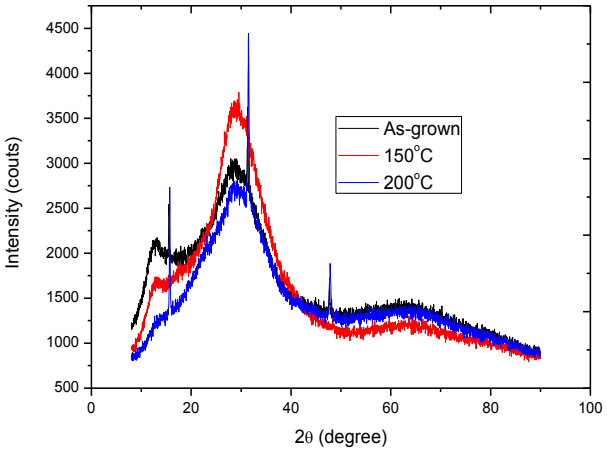

Fig. 2. XRD patterns of Cu_2S/Fe_2O_3 quaternary thin films.

The SEM images are characterized by grain sizes whose compactness and uniformity tend to increase with annealing temperature (Fig. 3-5). The SEM images reveal difference in surface texture and good film uniformity over significant surface area of a continuous phase. The variations in the morphology of the films showed that the annealing of the films affected the structure of the films. These findings are in agreement with the report of other authors [14].

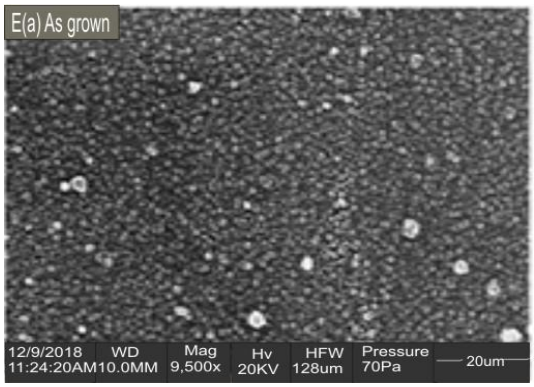

Fig. 3. SEM images of Cu_2S/Fe_2O_3 quaternary thin films for As-grown.

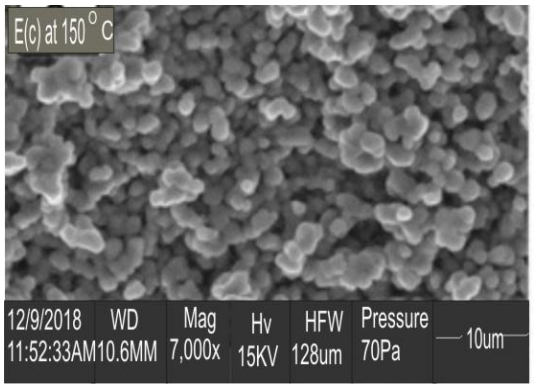

Fig. 4. SEM images of Cu_2S/Fe_2O_3 quaternary thin films for annealed at 150^oC.

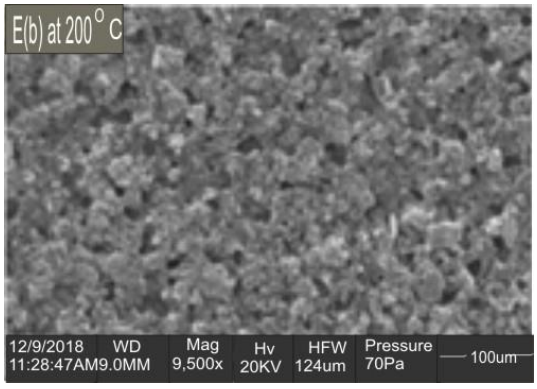

Fig. 5. SEM images of Cu_2S/Fe_2O_3 quaternary thin films for annealed at 200^oC.

The absorbance spectra reveals high absorbance in the UV region and low absorbance in the infrared region (Fig. 6). Enhanced absorbance is found in the neighbourhood of 300-400 nm. The absorbance generally decreases with wavelength and varies between 0.05-0.66 for as-grown, 0.05-0.60 for annealed at 150^{o}C and 0.06-0.65 for annealed at 200^{o}C. Our values agree with values reported by other authors for different thin films [15]. Within each wavelength, there is an appreciable increase in transmittance (Fig.7). All the film samples have maximum transmittance in the IR region and minimum in the UV region. These films agree fairly with report of films deposited on glass substrates prepared by chemical bath deposition technique, which were very high in the infrared region, with transmittance >85% [16, 17]. The high transmittance in the infrared region is desirable for use as coating materials in the construction of poultry houses. This

will facilitate the entrance of infrared light (heat) into the building for warming of young chicks. This has the potential to reduce the cost of energy consumption associated with the use of electric stoves, lambs and bulbs and at the same time reduce the hazards associated with high ultraviolet radiation. These findings are corroborated by the reports of other authors [18-20]. Enhanced reflection is seen in the neighbourhood of 300-350 nm. The reflectance decreases sharply with wavelength above 350 nm across the UV-VIS-NIR region (Fig. 8). Maximum reflectance of 20%, 24% and 21% were found for as-grown, annealed at 150^{o}C and 200^{o}C respectively.

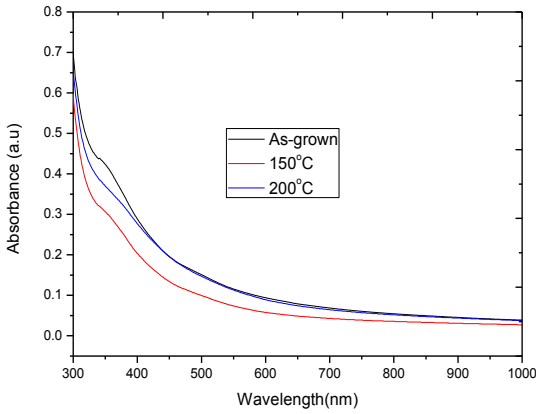

Fig. 6. Plot of Absorbance against Wavelength.

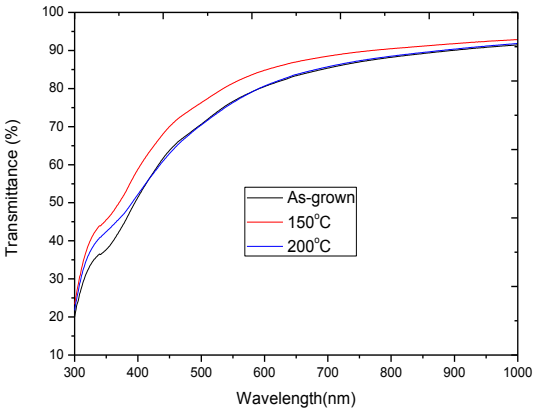

Fig. 7. Plot of Transmittance Against Wavelength.

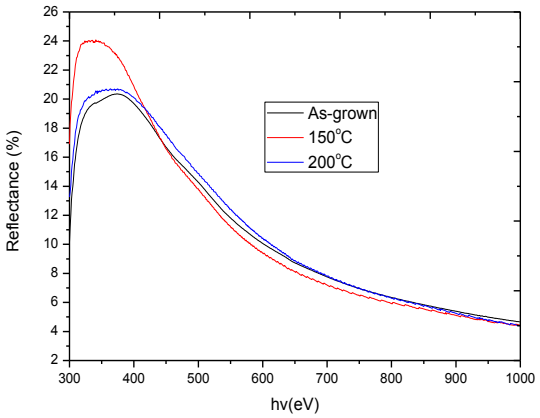

Fig. 8. Plot of Reflectance Against Wavelength.

The absorption coefficient increases with photon energy and varies from $0.1x10^6$ m^{-1} to $1.70x10^6$ m^{-1} (Fig. 9). The obtained values of the direct energy band gap estimated from the plots of $(\alpha hv)^2$ versus hv, are 3.75 eV, 3.80 eV and 3.85 eV for as-grown, annealed at 150 ^oC and 200 ^oC respectively (Fig. 10).

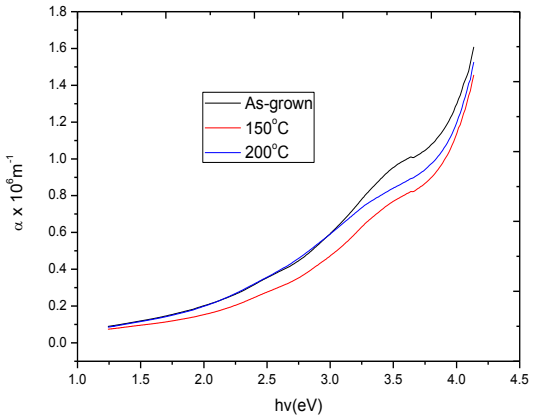

Fig. 9. Plot of Absorption Coefficient (α) versus hv.

The energy band gap increases with thermal annealing which agrees with the report of other authors [19]. Thin film solar cells consist of layers of different materials in thin film forms. In general, the solar cell consists of substrate o hold the thin film layers, transparent conducting oxide (TCO) to draw the current to the outer circuit, buffer layer to create the junction with the absorber layer with minimum absorption losses and to drive the generated carriers to the electrode, absorber layer for generating carriers on absorbing light with minimum transmission or reflection losses and metal contact layer as the bottom electrode. Buffer layer with a wider band gap could enhance the amount of light reaching the junction which is the main bottle neck in heterojunction solar cells. The Cu_2S-Fe_2O_3 thin films deposited here under various annealing temperature exhibit both high transparency and wide band gap energy and could be used for this purpose. Yet, another advantage is that recombination in wide band gap semiconductor is usually low and is a desirable attribute for use as buffer layer in heterojunction solar cell.

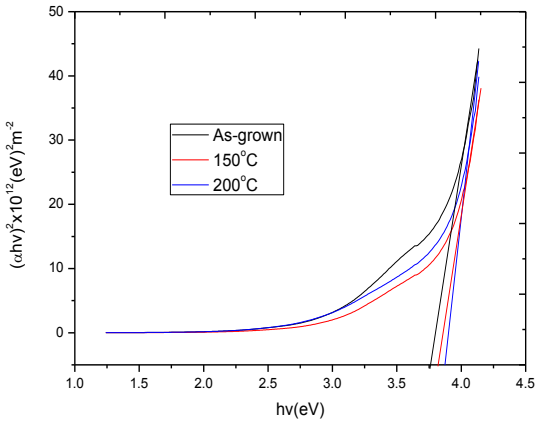

Fig. 10. Plot of $(\alpha hv)^2$ Versus hv.

The extinction coefficient, k varies in a similar manner with absorption coefficient, increasing with photon energy (Fig. 11). Maximum k values of 3.75, 3.25 and 3.40 were recorded for As-grown, annealed at 150 ^oC and 200 ^oC respectively. As observed in the plot of refractive

index (n) versus photon energy (hv) (Fig. 12), n varies from 1.0-1.1 for As-grown, 1.50-2.90 for annealed at 150 ^{o}C and 1.50-2.60 for annealed at 200 ^{o}C.

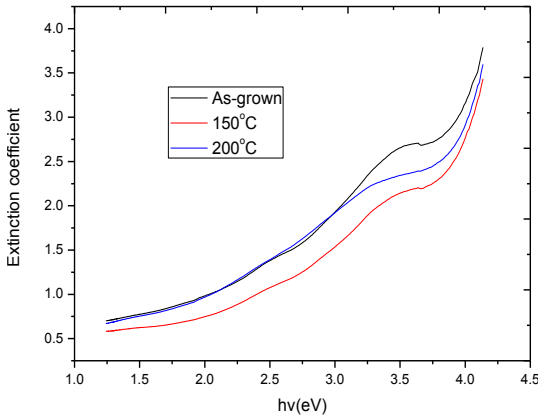

Fig. 11. Plot of Extinction Coefficient versus hv.

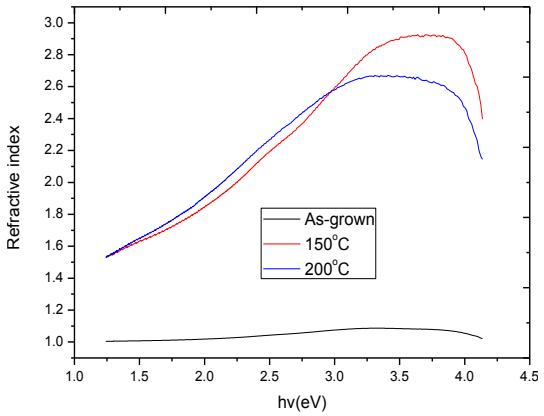

Fig. 12. Plot of Refractive Index versus hv.

The complex dielectric constant is a fundamental intrinsic property of the material. The imaginary part shows how a dielectric material absorbs energy from an electric filed due to dipole motion while The real part of dielectric constant shows how much the speed of light slows down in the material. The plots of real and imaginary parts of dielectric constant are shown in Figures 13 and 14 respectively. As observed in Fig. 13, ε_r varies in the same manner with n, differing only in magnitude. Maximum ε_r values are 1.0, 8.5 and 6.80 for as-grown, annealed at 150 ^{o}C and 200 ^{o}C respectively while the minimum values are 0.5, 5.5 and 4.5 for as-grown, annealed at 150 ^{o}C and 200 ^{o}C respectively. From Fig. 14, ε_i increases with photon energy across the entire UV-VIS-NIR regions. ε_i varies from 0.15 to 0.75 for as-grown, 0.20 to 1.65 for annealed at 150 ^{o}C and 2.05 to 1.55 for annealed at 200 ^{o}C.

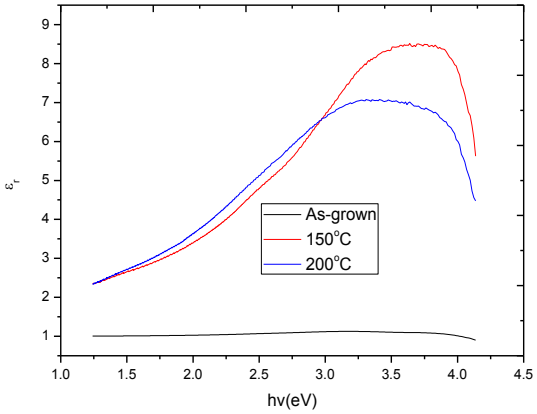

Fig. 13. Plot of Real Dielectric Constant (ε_r) Versus hv.

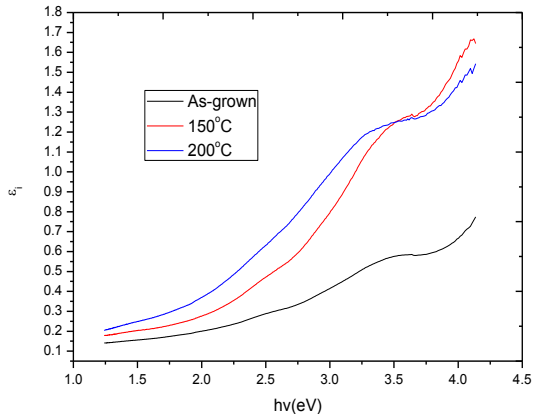

Fig. 14. Plot of Imaginary Dielectric Constant (ε_i) Versus Photon Energy (hv).

4. Conclusion

In this study, we have grown Cu_2S/Fe_2O_3 quaternary thin films on glass substrate by chemical bath deposition method. The deposited films were subjected to 150^o and 200^{o}C annealing temperatures. The optical and solid state properties of the films were investigated. It is found that all the optical parameters varied considerably with parameters of growth. In particular, the band gap blue shifted increasing from 3.75eV for as-grown to 3.80eV for annealed at 150^{o}C to 3.85eV for annealed at 200^{o}C. In view of the various wide band gap energy exhibited by the films, they are promising window materials for solar cell fabrication as well as optoelectronic applications.

References

[1] P. Parreira, J. Alloy Comp. 509, 5099 (2011); https://doi.org/10.1016/j.jallcom.2011.01.174
[2] C. Xu, Z. Zhang, Q. Ye, X. Liu, Chem. Lett. 32, 198 (2003); https://doi.org/10.1246/cl.2003.198
[3] P .K. Nair, M. T. S. Nair, J. Phys. D Apply. Phys. 24, 83 (1991); https://doi.org/10.1088/0022-3727/24/1/016
[4] S. L. Mammah, F. E. Opara, F. B. Sigalo, S. C. Ezugwu, F. I. Ezema, Annealing effect on the

solid state and optical properties of α-Fe2O3 thin films deposited using the Aqueous Chemical Growth (ACG) methods, 3, 793 (2012); https://doi.org/10.4236/msa.2012.311115

[5] B. Avijit, Pickard's Manual of Operative Dentistry, Oxford University Press Inc., New York, 89 (2011).

[6] A. S. Teja, P. Y. Koh, Progress in Crystal Growth and Characterization Matterials 55, 22 (2009); https://doi.org/10.1016/j.pcrysgrow.2008.08.003

[7] T. Marin, C. Nada, P. Matjaz, S. Zoran, M. S. Dragana, S. Vojstav, Journal of Alloys andCompounds 509, 7639 (2011).

[8] J. Singh, M. Srivastava, J. Dutta, P. K. Dutta, International Journal of Biological Macromolecules 48, 170 (2011); https://doi.org/10.1016/j.ijbiomac.2010.10.016

[9] M. Patil, D. Sharma, A. Dive, S. Mahajan, R. Sharma, Procedia Manufacturing 20, 505 (2018); https://doi.org/10.1016/j.promfg.2018.02.075

[10] A. G. Patil, A. P. Maharolkar, S. L. Patankar, A G Murugkar, International Journal of advanced Research in Basic and Applied Sciences, 62 (2017).

[11] C. D. Lokhande, B. R. Sankapal, S. D. Sarate, H. M. Pathan, M. Giersig, V. Ganeshan, Appl. Surf. Sci. 182, 413 (2001).

[12] I. Kazeminezhad, S. Mosivand, Phase transitions of electrooxidized Fe2O3 to α and γ-Fe2O3 nanopaticles using sintering treatment, (2014).

[13] M. Saadeldin, H. S. Soliman, H. A. M. Ali, K. Sawaby, Chem. Phys. B 23(4), 046803 (2014); https://doi.org/10.1088/1674-1056/23/4/046803

[14] F. I. Ezema, A. B. C. Ekwealor, R. U. Osuji, Super Ficies Vacio 21(1), 6 (2008).

[15] M. A. Manal, H. H. Noor, I. M. Hanaa, H. M. Ghuson, A. A. Kadhim, F. A. Ameer, Journal of Electron Devices 12, 761 (2012).

[16] P. E. Agbo, M. N. Nnabuchi, Chalcogenide Letters 8, 273 (2011). '

[17] P. E. Agbo, G. F. Ibeh, S. O. Okeke, J. E. Epke, Communications in Applied Sciences 1(1), 38 (2013).

[18] R. A. Chikwenze, M. N. Nnabuchi, Chalcogenide Letters 7, 401 (2010).

[19] C. Augustine, M. N. Nnabuchi, Materials Research Express 5, 1 (2018).

[20] P. N. Kalu, D. U. Onah, P. E. Agbo, C. Augustine, R. A. Chikwenze, F. N. C. Anyaegbunam, C. O. Dike, Journal of Ovonic Research 14, 293 (2018).